

Epitaxial growth of binary alloy nanostructures

S. Heinrichs,¹ W. Dieterich,¹ and P. Maass²

¹*Fachbereich Physik, Universität Konstanz D-78457 Konstanz, Germany and*

²*Technische Universität Ilmenau - Institut für Physik, D-98684 Ilmenau, Germany*

(Dated: July 11, 2006)

Stochastic growth of binary alloys on a weakly interacting substrate is studied by kinetic Monte Carlo simulation. The underlying lattice model relates to fcc alloys, and the kinetics are based on deposition, atomic migration with bond-breaking processes and exchange processes mediated by nearest neighbor hopping steps. We investigate the interrelation between surface processes and the emerging nonequilibrium structure at and below the growing surface under conditions where atoms in the bulk can be regarded as immobile. The parameters of the model are adapted to CoPt₃ alloys. Growing nanoclusters exhibit an anisotropic short range order, primarily caused by Pt segregation at the surface. The overall structural anisotropy depends on both Pt surface segregation and cluster shape, and can explain the perpendicular magnetic anisotropy (PMA) recently measured in CoPt₃ nanoclusters on a van der Waals substrate. The onset of L1₂ ordering in the cluster is induced by surface processes. The same kinetic model is applied also to continuous thin films, which in addition can exhibit a small bulk contribution to PMA.

PACS numbers: 81.15.Aa, 68.55.Ac

I. INTRODUCTION

Molecular beam epitaxy (MBE) has become an important tool to prepare ultrathin films and nanostructures in nonequilibrium, frozen-in states that show novel properties distinctly different from the equilibrium bulk phases. Theoretically, an important question is how to relate the structural characteristics of the growing material to the incoming flux, substrate temperature, adatom diffusion coefficients and adatom interactions. Successive stages of growth, nucleation and island formation in the submonolayer regime,¹ second layer nucleation,^{2,3} growth of three-dimensional clusters and emerging film morphologies, are fairly well understood for the one-component case, i.e. for deposition of only one species of atoms.^{4,5} By contrast, nonequilibrium alloy nanostructures produced by codeposition of two or more atomic species can display a variety of additional new phenomena that are only partly understood up to now. From the viewpoint of theoretical modelling, this is true in particular for metallic nanoalloys, which recently became of great interest from the experimental and technological viewpoint.⁶

In many MBE experiments the substrate temperature is chosen sufficiently low so that atomic configurations in the interior of a growing cluster or film can be considered as frozen. Structural relaxation then takes place only among lower-coordinated atoms within the growth zone. Specific to binary systems are the following questions:

- i) Suppose that one atomic species tends to segregate at the surface. What is the emerging bulk structure upon further deposition burying a segregated surface layer?
- ii) How large is a possible anisotropy in the frozen short-range order, i.e. a difference in the alloy structure between the lateral and the perpendicular (growth) direction?

- iii) To what extent can diffusion processes limited to the near-surface region give rise to long-range order in the bulk of an ordering alloy at temperatures below the equilibrium order-disorder transition point?
- iv) In the case of magnetic alloys, what are the magnetic properties associated with the non-equilibrium short or long-range order? This question is central in the ongoing search for materials that display a stable perpendicular magnetic anisotropy (PMA), which is useful for the development of high-density magnetic storage media. Under this viewpoint fcc-alloy systems of Co-Pt,^{7,8} Fe-Pt⁹ or Fe-Co¹⁰ draw great attention in current investigations.

Here we report on answers related to these problems, based on kinetic Monte Carlo (KMC) simulations of a statistical model for binary fcc alloys of composition AB₃, with emphasis on CoPt₃ alloys.

MBE-grown nanoclusters of CoPt₃ on a van der Waals WSe₂ substrate were found recently to exhibit PMA at room temperature and below the onset of L1₂-ordering.⁷ The origin of PMA is thought to lie in a structural anisotropy induced by the growth process, strong enough to overcome the dipolar form anisotropy favoring in-plane magnetization. The model we use is based on effective chemical interaction and kinetic parameters extracted, respectively, from known equilibrium properties of CoPt₃^{11,12} and from separate diffusion measurements.¹³ The dependence of the magnetic anisotropy on the local structure is represented by a sum over bond contributions, with nearest neighbor Co-Pt bonds as the dominant part. The associated bond anisotropy parameter is deduced from magnetic measurements on Co-Pt multilayer systems.¹⁴ Within this model it was shown that Pt surface segregation and cluster shape effects can explain the occurrence of PMA in some

temperature window, followed by the evolution of L1₂-order at higher temperatures.¹⁵ In this paper we present further details on cluster structures and extend our previous investigations to homogeneous films.

In section II we introduce our kinetic model, based on random deposition and subsequent hopping moves of A and B atoms to neighboring sites of an fcc lattice. Hopping rates are derived from the energetics in the specific environment of each atom. To our knowledge, most prior KMC simulations of three-dimensional growth of binary systems were in the framework of solid on solid (SOS) models,¹⁶ which are not well suitable to describe cluster shapes and facetting in a realistic way. In very recent work the growth of CoPt₃ films was simulated, using a more realistic tight binding, second moment approximation to the interatomic interaction potential.¹⁷ Segregation of Co-atoms to step edges on the growing surface was predicted, which leads to in-plane Co-clustering.¹⁸ By this the authors were able to explain PMA in disordered films, known from previous measurements⁸ to occur at elevated temperatures ($T \gtrsim 500\text{K}$).

Our model, based on effective nearest neighbor couplings, allows for fully three-dimensional kinetics, a feature which is important in simulations of cluster growth and L1₂ ordering. It yields cluster facets in agreement with those observed in experiments and consistently accounts for mass transport along the cluster side and top facets. Both height and lateral growth largely relies on interlayer diffusion that starts from adatoms on the substrate, reaching higher layers along side facets. The present model automatically entails step edge barriers, dissociation from the surface and the possibility of vacancy diffusion in the bulk. It is less comprehensive than recent simulations of island formation in compound semiconductors, which are based on extensive electronic density functional calculations for energy barriers of the processes involved. These calculations, however, were so far limited to the submonolayer regime.¹⁹ Section IIB also describes a phenomenological relationship between the local contributions to the magnetic anisotropy and atomic short range order within a bond picture.

The anisotropic short range order and associated magnetic properties of clusters up to 4000 atoms are presented in section III, and are discussed in detail in terms of surface segregation and cluster shape. The same algorithm is applied in section IV to thin films. In addition to surface -induced PMA a bulk contribution is identified which, however, is too small to account for the measured PMA in thick films. Further conclusions are drawn in section V.

II. SIMULATION MODEL

A. Interactions and Kinetics

Our model starts from a reference fcc lattice with nearest neighbor distance a in a cubic simulation box

$L \times L \times L_z$ where sites can be occupied by an atom of type A (Co), B (Pt), or by a vacancy V. In contrast to models with a small concentration of vacancies and fixed shape of the sample, most of the simulation box considered here consists of vacancies representing the free space in the vicinity of the cluster. This allows for an unconstrained evolution of the cluster morphology. Effective interactions between A and B atoms are restricted to nearest neighbor pairs. This simplified description already captures essential statistical properties of ordering fcc alloys, including the phase diagram which displays L1₂ and L1₀ ordered structures in the vicinity of the AB₃ and AB-composition, respectively.^{12,20}

Bond energies between the different atomic species are denoted by V_{AA} , V_{AB} and V_{BB} . The linear combinations $I = \frac{1}{4}(V_{AA} + V_{BB} - 2V_{AB})$, $h = V_{BB} - V_{AA}$ which acts as a surface field, and $V_0 = (V_{AB} + V_{BB})/2$ control the bulk order-disorder transition temperature, the degree of surface segregation of B-atoms, and the average bond energy in the L1₂ ordered state. Parameter values are adjusted to reproduce equilibrium properties of CoPt₃: (i) The transition from the disordered to the L1₂-structure occurs at $T_0 \simeq 958\text{K}$,²¹ which is related to I by $k_B T_0 \simeq 1.83I$.²² Setting $I = 1$, our energy unit becomes $k_B T_0/1.83 = 45\text{meV}$, corresponding to 523 K. (ii) The observed Pt surface segregation of nearly 100%,¹¹ caused by the larger size of Pt relative to Co, is compatible with $h \gtrsim 4$; here we choose $h = 4$ in most of our calculations. (iii) At temperatures of interest, the mobility of atoms is effectively restricted to the film or cluster surface so that their typical coordination is between 3 (for an adatom on top of a terrace) and 7 (for an atom attached to a step edge). Parameters for a variety of corresponding processes were calculated for Pt within electronic density functional theory (DFT).²³ Different processes were classified according to the number of broken bonds, and the average bond energy yielded $V_0 \simeq -5$, which we use here. Clearly, these bond energies are to be understood as effective energies since real interactions can extend to several neighbors.²⁴

Experiments for nanoclusters of CoPt₃ were performed on a WSe₂ (0001) substrate surface,⁷ which is of the van der Waals type. The interaction with the substrate is modelled by a weak attractive potential, represented by an additional energy V_s for atoms in the first layer. In the cluster simulations we choose $V_s = -5$. Compared to an fcc Pt (111) surface with three bonds of typical strength V_0 , this amounts to about 1/3 of the energy of a single Pt-Pt bond.

The total flux F of incoming atoms is taken as $F = 3.5$ monolayers/s. Additional parameters needed to describe the kinetics of the system are the transition state energy U_t and the attempt frequency ν for atomic moves. These values are known from diffusion experiments¹³ of Pt on Pt (111) surfaces as $\nu = 8.3 \cdot 10^{11} \text{ s}^{-1}$ and $U_t \simeq 5$. The resulting diffusion coefficient is $D/a^2 = (\nu/4)e^{-U_t/k_B T}$ for moves without change in energy.

The rate for an elementary hopping process with a final

energy E_f and initial energy E_i is chosen to be

$$w_{if} = \nu e^{-U_t/k_B T} \min(1, e^{-(E_f - E_i)/k_B T}) \quad (1)$$

which fulfills the condition of detailed balance. As long as the general kinetics are concerned, characterized by the tendency of the system to approach thermal equilibrium, the specific form (1) of the hopping rates should not be of crucial importance.

In many cases,^{25,26} including Co deposited on Pt(111), adatoms on the top of a terrace or at step edges can exchange positions with an atom underneath in one concerted move. In comparison to single atom moves considered so far, a larger binding energy has to be overcome in order to effect such a simultaneous move of two particles. However, at the same time the transition state energy can be reduced because of the higher coordination in the transition state configuration. Direct exchange processes are found for Co deposited on Pt(111) over a wide temperature range 250–520 K.^{25,26} They are especially frequent for low-coordinated atoms on top of terraces (with coordination 3) or at step edges (with coordinations 4 or 5). We therefore include direct exchange processes between unlike atoms in the simulation. The corresponding rate involves an exchange barrier U_x that adds to the migration barrier U_t , while initial and final energies are taken into account as before. These exchange processes, however, are allowed only if one atom has a coordination in the range 3–5 and the other one in the range 8–10. Let us remark that the activation energy for exchange diffusion of Pt on Pt (100) is just 470 mV,²⁷ which is almost the same as the total barrier $U_t + U_x$ when $U_x = 5$, as used in most of our computations described below.

The time evolution in our simulation is determined by a rejectionless continuous time MC-algorithm that generates realizations of the master equation describing the growth kinetics. Each simulation step consists of: (i) incrementing the time by an interval Δt drawn from an exponential distribution with mean $\langle \Delta t \rangle = (\sum_f w_{if})^{-1}$, (ii) executing a process $i \rightarrow f$ with probability proportional to its rate w_{if} , (iii) updating of rates of processes affected by the moving atom.

The simulation box consists of 15 layers with 1440 lattice sites each. To generate an isolated cluster attached to the weakly binding substrate, we start from a seed with 5 atoms on the surface. For the deposition rate $F = 3.5$ ML/s used in most simulations and temperatures $T > 0.5$, the distance between clusters, which would be observed by self-organized nucleation, exceeds the box size. This could be effectively accounted for by increasing the deposition rate at the boundary of the box to match the extra flux of atoms deposited within the typical capture zone of an island. However, in order to reduce the number of parameters, we deliberately kept the deposition rate constant for all temperatures.

An example of a typical cluster with $N = 2000$ atoms obtained in the KMC simulations is shown in Fig. 1. The top facet has (111) orientation as expected for the (111) substrate, and side facets are of (111) and (100)

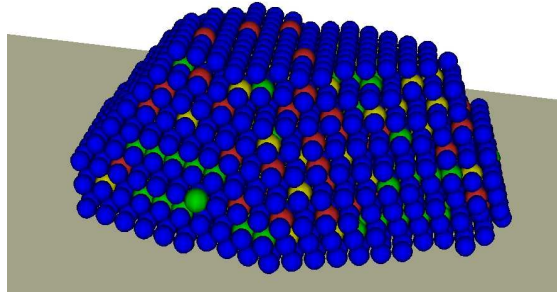


FIG. 1: A typical cluster configuration with 2000 atoms for $h = 4$, $T = 1.2$ and $U_x = 0$. Pt atoms are marked in blue and Co atoms are marked in different colors depending on the number of nearest neighbor Pt atoms: if more (less) Pt atoms are found out of plane than in plane the atom is marked in green (yellow); otherwise it is marked in red. Facets with sixfold {111} and fourfold {100} symmetry can be clearly distinguished.

TABLE I: Parameters used in the simulation. All energies are given in units of $k_B T_0 / 1.83 = 45$ meV.

I	h	V_0	V_s	U_t	U_x	ν
1	4	-5	-5	5	5	$8.3 \cdot 10^{11} \text{ s}^{-1}$

type. The surface shows strong Pt segregation. Similar to the experiments,⁶ the aspect ratio of lateral to height dimension of the cluster is about 3:1. At the temperature $T = 1.2$, the ratio $D/Fa^4 \simeq 2 \cdot 10^{10}$, and the realization of the growth process implied $3.3 \cdot 10^{10}$ elementary processes. A simple MC algorithm which generates equivalent dynamics, but is not rejection free, can be estimated to require about $N^2 D / (a^4 L^2 F) \simeq 6 \cdot 10^{13}$ trials for elementary moves, i.e. about 2000 times more than the algorithm used here. This ratio increases further at lower temperatures, since bond breaking processes will acquire lower rates and consequently contribute to larger time increments Δt . Subsequent equilibration of the clusters under zero flux during a multiple of the deposition time did not induce significant changes in the cluster configurations and will therefore be ignored in the following.

To generate homogeneous films (where the width of the interfacial growth zone is much smaller than the average film thickness), discussed in section IV, we choose a stronger surface potential $V_s = -15$ which guarantees complete wetting in the first layer in the temperature range considered.

B. Structure-induced magnetic properties

In CoPt₃-alloys magnetic moments are mostly due to the Co atoms, with $\mu^{\text{Co}} \simeq 1.7\mu_B$,^{8,28} while Pt atoms carry a comparatively small induced moment μ^{Pt} of

about $0.3\mu_B$, which has been shown to depend on the actual atomic environment.¹² Hybridization of d-electrons between neighboring Co and Pt atoms and a strong spin-orbit interaction near the Pt sites lead to a magnetic anisotropy that tends to align the Co moment along the Co-Pt bond direction. In the following we adopt a bond picture as in earlier work on bulk systems,^{29,30} where the structural part of the magnetic anisotropy, H_A , is expressed as a sum over bonds $\langle i, \delta \rangle$ that connect a Co atom with moment μ_i^{Co} at site \mathbf{R}_i with a species α ($\alpha = \text{Co, Pt, V}$) at a site $\mathbf{R}_i + \delta$,

$$H_A = - \sum_{\langle i, \delta \rangle} \sum_{\alpha} A^{\text{Co}\alpha} (\mu_i^{\text{Co}} \cdot \delta)^2 / (|\mu_i^{\text{Co}}| |\delta|)^2 \quad (2)$$

By δ we have denoted the 12 possible nearest neighbor bond vectors in the fcc lattice. Note that this anisotropy term naturally entails both surface and bulk contributions by considering vacancies as a possible neighbor species.

The parameters $A^{\text{Co}\alpha}$ are the anisotropy energies associated with a Co- α bond. These are deduced from experiment and the term $\alpha = \text{Pt}$ gives the dominant contribution. Note that for saturated magnetization a nearest neighbor contribution to the anisotropic part of dipole-dipole interactions has exactly the same form, so that this contribution is included already in the coefficients $A^{\text{Co}\alpha}$. The isotropic part of the exchange interactions only leads to a small renormalization of chemical interactions.

Equation (2) provides a relationship between a given atomic structure, to be obtained from simulations, and the magnetic anisotropy energy. Magnetic anisotropies for disordered alloys, including Co-Pt alloys, have been obtained by microscopic calculations based on the KKR-CPA method.³¹ Although less accurate in principle, the local expression (2) here allows us to relate effects in the atomic short range order to the anisotropy energy in a direct way. Note that 2nd order contributions of the anisotropy in the direction cosines as in eq. (2) do not yield a magneto-crystalline anisotropy in an fcc lattice occupied by a single species. Additional bulk contributions are of 4th order and generally much weaker than the magnetic anisotropy in lower symmetry configurations to be considered here.

Several observations support the bond picture underlying eq. (2) as a reasonable approximation. Magnetic torque and magneto-optical Kerr-effect measurements on Co-Pt multilayers show that the anisotropy energy in these systems is dominated by an interfacial contribution connected to Co-Pt bonds. Detailed measurements of multilayers yield $K^{\text{CoPt}} = 0.97 \text{ mJ/m}^2$ for (111) orientation and $K^{\text{CoPt}} = 0.59 \text{ mJ/m}^2$ for (100) orientation.^{14,32} Considering the different angles of bonds to the surface and the different packings, eq. (2) indeed can reproduce this difference with one consistent value for $A^{\text{CoPt}} \approx 250 \mu\text{eV}$ per Co-Pt bond.³⁶ Hence, on a semi-quantitative level, anisotropy energies of Co-moments in different chemical environments are consistent with a superposition of bond contributions and a bond energy

A^{CoPt} as given above.

Similarly, from measurements on Co-vacuum interfaces^{37,38} and theoretical investigations of a freely standing Co-monolayer³⁹ we estimate $A^{\text{CoV}} \simeq -67 \mu\text{eV}$. The remaining parameter is A^{CoCo} for which we retain only the nearest neighbor dipolar contribution as discussed above. Using $\mu^{\text{Co}} = 1.7\mu_B$ and $|\delta| = 2.72 \text{ \AA}$ in CoPt_3 , this yields $A^{\text{CoCo}} = 23 \mu\text{eV}$.

It is now straightforward to express the part of the anisotropy energy caused by local chemical order,

$$E_s = H_A \{\mu \text{ in plane} \} - H_A \{\mu \text{ out of plane} \} \quad (3)$$

in terms of the numbers of Co- α bonds in plane, $n_{\parallel}^{\text{Co}\alpha}$, and out of plane, $n_{\perp}^{\text{Co}\alpha}$. Using a site occupation number representation and the condition that occupation numbers for the three species α add up to unity at each site, (3) can be brought into the form

$$E_s = \sum_{\alpha=\text{Co,Pt}} E_s^{\text{Co}\alpha} = \frac{N}{2} \sum_{\alpha=\text{Co,Pt}} (A^{\text{Co}\alpha} - A^{\text{CoV}}) P^{\text{Co}\alpha} \quad (4)$$

with structural anisotropy parameters

$$P^{\text{Co}\alpha} = \frac{1}{N} (n_{\perp}^{\text{Co}\alpha} - n_{\parallel}^{\text{Co}\alpha}). \quad (5)$$

These parameters enter as the primary structural characteristics related to the magnetic anisotropy.

In addition one has to take into account the magnetic form anisotropy due to dipolar interactions. Dipolar sums for a given cluster with saturated magnetic moment \mathbf{M}_s are carried out using moments for Co and Pt as given before. By E_{dip} we denote the difference in dipolar energies for \mathbf{M}_s parallel and perpendicular to the substrate, respectively. The anisotropy within the substrate plane turns out to be negligibly small because of the approximate 3-fold symmetry of cluster shapes. Nearest neighbor dipole-dipole interactions were already incorporated in the quantity E_s , as described above. The total magnetic anisotropy energy of a cluster is then given by

$$E_{\text{tot}} = E_s + E_{\text{dip}} \quad (6)$$

Dipolar interactions generally favor in plane magnetization of thin films and clusters, $E_{\text{dip}} < 0$. For thin homogeneous films, $E_{\text{dip}} = -(\mu_0/2)M_s^2$.

As mentioned above and supported by the above estimates, the term $\alpha = \text{Pt}$ dominates expression (4). PMA hence requires P^{CoPt} to be sufficiently large that E_s can overcome the negative dipolar energy.

III. CLUSTERS

The two anisotropy parameters P^{CoPt} and P^{CoCo} defined in (5) are shown in Fig. 2 as a function of temperature for clusters consisting of 1000 atoms. The solid lines connect data points for different values of the extra

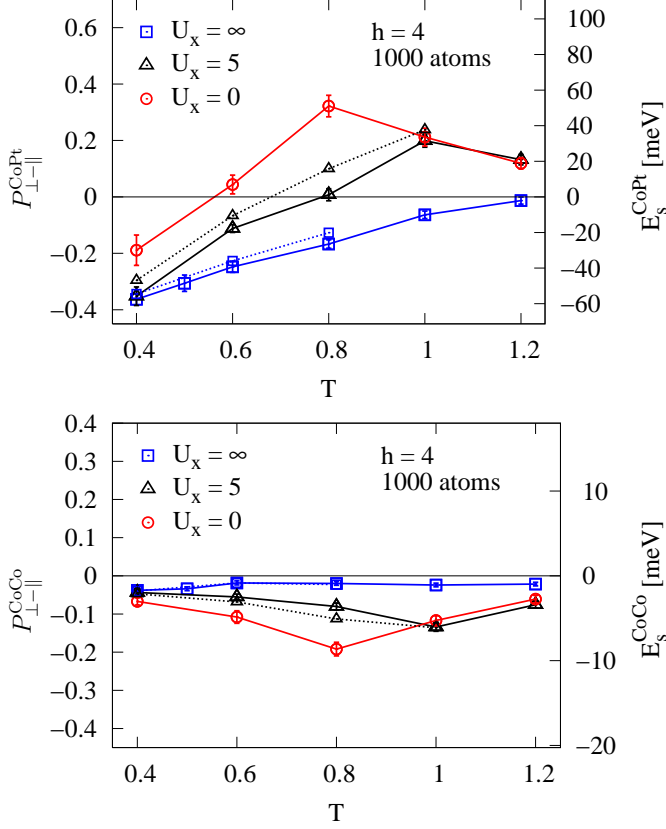


FIG. 2: Structural anisotropy parameters $P_{\perp-\parallel}^{\text{CoPt}}$ (upper panel) and $P_{\perp-\parallel}^{\text{CoCo}}$ (lower panel) and corresponding structural anisotropy energies. The dashed lines correspond to data obtained with a deposition rate of $F = 0.35$ ML/s, which is 10 times smaller than the rate used for the full lines.

barrier for exchange processes U_x , and for a flux $F = 3.5$ ML/s. In the absence of exchange processes ($U_x = \infty$) both anisotropy parameters are smaller than zero for all temperatures, leading to a preference of in-plane magnetization. The reason is that the clusters are relatively flat and that surface segregation of Pt is weak because of kinetic suppression. As a consequence, in the surface of a cluster there exist more Co-Pt bonds in-plane than out-of-plane, while atoms in the inner part of the cluster give essentially no contribution to P . The flat cluster shape, on the other hand, would favor PMA if strong Pt segregation as realized at equilibrium could build up.

Indeed, when including exchange processes, Pt segregation gets enhanced considerably and P can become positive. Actually, the cluster displayed in Fig. 1, showing pronounced Pt segregation to the (111) and (100) facets, was computed with $U_x = 0$. As seen from Fig. 2a, for $U_x = 0$, P^{CoPt} changes sign near $T = 0.58$ and reaches a maximum at an optimum temperature $T_{\text{max}} \simeq 0.8$. Conversely, $P^{\text{CoCo}} < 0$ for all parameters, which leads to a small reduction of the sum (4) relative to its leading term $\alpha = \text{Pt}$, see Fig. 2b.

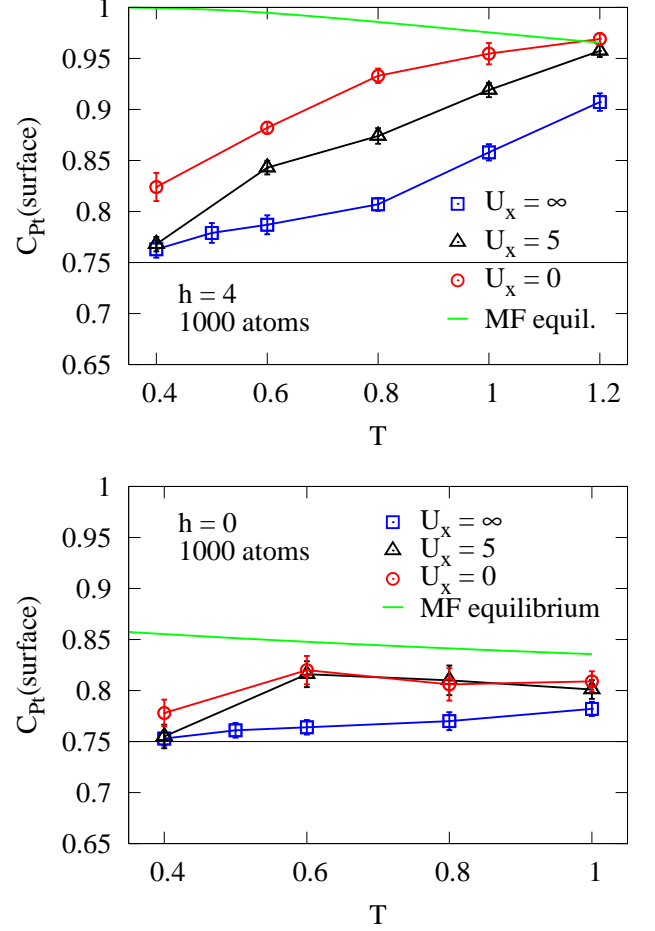


FIG. 3: Concentration of Pt atoms in the outer shell of clusters for $h = E_{\text{PtPt}} - E_{\text{CoCo}} = 4$ in the upper panel and $h = 0$ in the lower panel. The uppermost lines result from the mean field equations (7) and (8).

The third set of data in Fig. 2 (triangles) refers to $U_x = 5$. This means that the activation energy for direct exchange is twice the diffusion barrier. Yet exchange processes have an important influence as they still can render P^{CoPt} positive. The onset of a positive P^{CoPt} and the temperature where P^{CoPt} takes its maximum are shifted to somewhat higher values than in the case $U_x = 0$. Fig. 2 also contains data for the flux $F = 0.35$ ML/s. The reduction of F by one order of magnitude apparently leads to a small increase of P^{CoPt} .

Investigating the mechanism of PMA in more detail we find that the sign of P^{CoPt} is determined by two major factors which show opposing trends in their temperature dependence. These are the degree of Pt surface segregation and the cluster shape, which we now discuss in more detail.

The concentration C_{Pt} of Pt-atoms in the outer shell of a 1000 atom cluster is plotted in Fig. 3, again for a flux $F = 3.5$ ML/s and three values of U_x . As dis-

cussed above, the observed degree of Pt surface segregation is generally smaller than in the equilibrium case because of kinetic hindrance: During growth, the time for attaining equilibrium through exchange and diffusion processes is limited due to continuous incorporation of newly deposited atoms. Fig. 3 reveals that both direct exchange processes and an increasing temperature act towards restoring equilibrium, i.e. they facilitate Pt surface segregation.

Clearly, a large C_{Pt} in the topmost layer leads to an enrichment of Co-atoms in the layer underneath. Therefore, for oblate cluster shapes with more surface area oriented in the $[111]$ direction than in directions perpendicular to $[111]$, a sufficiently strong segregation of Pt to the surface will induce a positive sign of P^{CoPt} . This favors PMA, even for a disordered structure within the cluster interior. Furthermore, the weakly binding van der Waals substrate also allows for segregation towards the substrate during growth, effectively doubling the available surface with favorable orientation.

It should be noted that segregation of the majority atoms (Pt) can be observed even when the parameter $h = V_{PtPt} - V_{CoCo}$ controlling segregation is zero. This can be understood from a mean-field argument that counts bonds in a slab with a free (111) surface: for a random fcc alloy structure, the exchange of a Co-atom at the surface with a Pt-atom in the bulk allows the system to lower its energy on average by $3I$, so that the surface concentration C_{Pt} will exceed the stoichiometric concentration, see Fig. 3. By contrast, for a fully $L1_2$ ordered alloy the stoichiometric composition at the surface yields the lowest energy.

In order to give a more quantitative estimate of segregation, we consider a mean field model that consists of three completely filled (111) layers of atoms. The first layer is the free surface and the third one has fixed stoichiometric composition. Exchange processes are allowed between the outermost two layers. This model takes into account the almost non-existent bulk diffusion within a cluster, which results in an increased concentration of Co in the second layer impeding further exchange. The internal energy term per atom for a given Co concentration in the first layer $C_{Co,1}$ can be expressed in the case of 1:3 stoichiometry as

$$U = 6V_0 - \frac{3}{16}h(1-4C_{Co,1}) + \frac{3}{2}I(1-C_{Co,1}+4C_{Co,1}^2). \quad (7)$$

The energy minimum at $T = 0$ is attained for $C_{Co,1} = \frac{1}{8}(1 - h/(2J))$ clearly predicting segregation for $h = 0$.

The entropy is

$$S = -\frac{k_B}{2} \sum_{\alpha=Co,Pt} \sum_{z=1}^2 C_{\alpha,z} \ln C_{\alpha,z}. \quad (8)$$

Minimizing the free energy $F = U - TS$ then yields the equilibrium concentration of Co and Pt in the first layer. The corresponding results for the Pt concentration are displayed in Fig. 3. Including the entropy term leads to

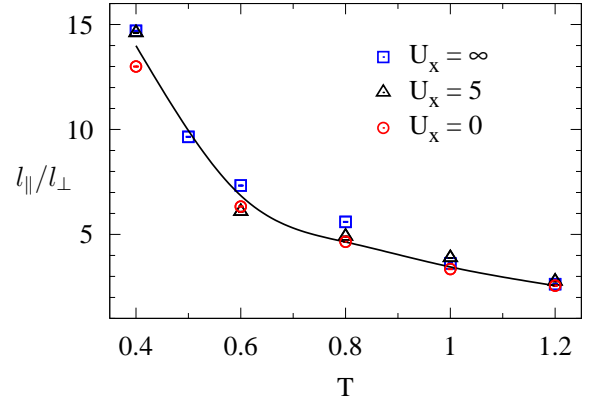


FIG. 4: Cluster shape represented by the ratio of gyration radii l_{\parallel}/l_{\perp} (with line as guide to the eye). Decreasing values signify the transition from oblate to spherically shaped clusters.

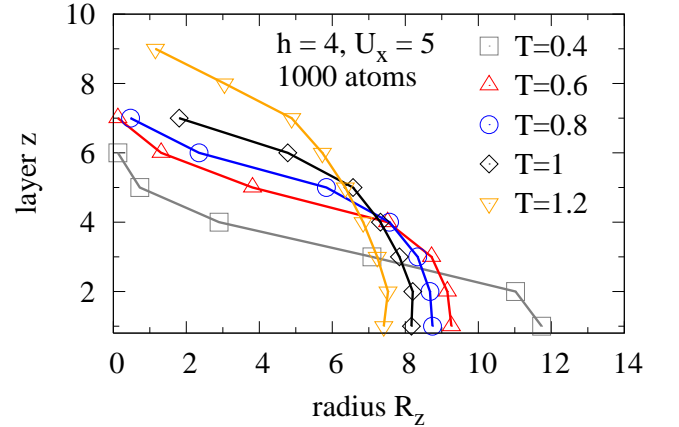


FIG. 5: Number of atoms per layer N_z represented with a radius $R_z = \sqrt{N_z/\pi}$ and averaged over 20 realizations of the growth process. Layer one is the bottom layer on the (111) substrate.

a decrease in Pt concentration in the outer shell with increasing temperature and restores the stoichiometric concentrations in the limit of high temperatures. Such a negative slope with temperature is reproduced in the simulations for $h = 0$ when exchange processes are included, but not in the simulations for $h = 4$ and $h = 0$ without exchange processes. The positive slope of simulated segregation values with temperature indicates that segregation differs from thermal equilibrium due to kinetic limitations. This model also does not account for the portions on the cluster surface which are not flat.

The second factor important for PMA is the cluster shape. An increasing temperature drives the shape closer to the equilibrium shape which is less oblate. This is seen from the aspect ratio l_{\parallel}/l_{\perp} of the gyration radii of clus-

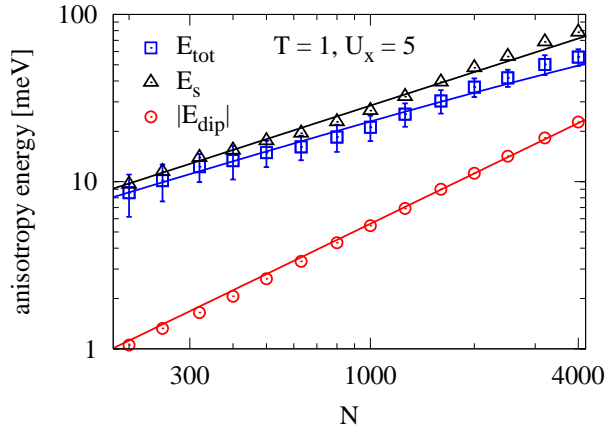


FIG. 6: Scaling plot of surface E_s and bulk E_{dip} contributions to the magnetic anisotropy $E_{\text{tot}} = E_s + E_{\text{dip}}$ as a function of cluster size N . The lines fitting E_s and E_{dip} have slope $2/3$ and 1 respectively. The line through E_{tot} is given by $E_{\text{tot}} = K_s N^{2/3} - K_{\text{dip}} N$, where the prefactors K_s and K_{dip} are obtained from the fits to E_s and E_{dip} .

ter sizes in the direction parallel and perpendicular to the substrate, shown in Fig. 4. Cluster shapes are parameterized in more detail in Fig. 5. The atomic layer z contains N_z atoms and has an effective radius $R_z = \sqrt{N_z/\pi}$. The figure displays the connection between z and R_z for a series of temperatures. It clearly shows the evolution of cluster shapes from oblate to almost a half-sphere as temperature is increased. In this way temperature effects in the cluster shape counteract the temperature dependent, segregation induced PMA. The result is the existence of a certain temperature window where PMA prevails, in agreement with experiments.^{6,7}

The discussion so far makes it clear that PMA essentially emerges as a surface effect. This suggests that $n_{\perp}^{\text{CoPt}} - n_{\parallel}^{\text{CoPt}} \sim N^{2/3}$, and accordingly $P^{\text{CoPt}} \simeq N^{-1/3}$. As shown by the solid line in Fig. 6, this behavior is well obeyed by the simulated data (triangles).

Combination of our results for P^{CoPt} with (4) yields the structural part of the anisotropy energy. Adding the dipolar energy (see section II) we obtain the total anisotropy energy (6), which can be written as

$$E_{\text{tot}} = K_s N^{2/3} - K_{\text{dip}} N \quad (9)$$

The temperature dependence of E_{tot} is shown in Fig. 7 for different U_x and $N = 10^3$ atoms. An optimal temperature where E_{tot} is maximum can clearly be identified. For example, for $U_x = 5$ we have $T_{\text{max}} \simeq 1$. Fig. 6 contains a double-logarithmic plot of E_{tot} as a function of N at $T = 1$, $U_x = 5$. From E_s and E_{dip} we obtain $K_s \simeq 285 \mu\text{eV}$ and $K_{\text{dip}} \simeq 5.6 \mu\text{eV}$. The line for E_{tot} in Fig. 6 represents the expression (9) and, upon extrapolation to larger N -values, predicts the existence of an optimal cluster size for PMA, which is $N_{\text{opt}} \simeq 4 \cdot 10^4$. PMA is expected to disappear when $N \simeq 1.3 \cdot 10^5$.

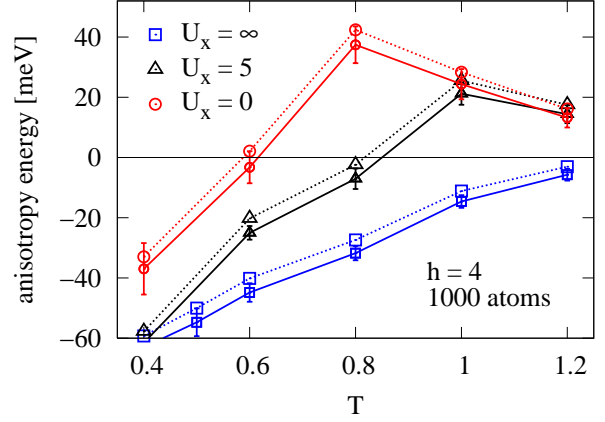


FIG. 7: Magnetic anisotropy energies E_{tot} (solid lines) and E_s (dashed lines) as a function of temperature for different values of the additional barrier U_x for exchange processes (no exchange processes for $U_x = \infty$). E_{tot} also includes the form anisotropy from dipolar interactions, while E_s only contains the bond contributions (with inclusion of the nearest neighbor part of the dipolar interactions).

Experimental values for E_{tot} for two different cluster sizes can be inferred by measurements of the blocking temperature using SQUID devices.⁷ For clusters with $N = 300$ at room temperature ($T = 0.56$), this leads to the estimate $E_{\text{tot}} \simeq 2.8 \text{ meV}$. Similarly, $E_{\text{tot}} = 3.4 \text{ meV}$ for $N = 1200$ at 573 K ($T = 1.1$). In a different set of experiments at $T = 0.56$, granular nanostructures (dense covering of surface, but not touching) with similar lateral size of 3 nm were obtained with considerably larger anisotropy constants $K \simeq 13 \mu\text{eV}$ per atom.⁷ In our simulation model values $E_{\text{tot}} \lesssim 12 \text{ meV}$ for $N = 300$ and $E_{\text{tot}} \lesssim 20 \text{ meV}$ for $N = 1200$ are found for $T \gtrsim 0.9$. The comparison shows that the experimentally observed values of the anisotropy energy lie within the ranges predicted by the model. The degree of agreement with experiment must be regarded as satisfactory in view of the uncertainties in the analysis of experiments and the simplifying assumptions in our model. One should also note the slower deposition rate in the experiments with $F = 0.02 \text{ ML/s}$, compared to $F = 3.5 \text{ ML/s}$ used in most simulations. An effect of slower deposition rates in the simulations can be seen in Fig. 2.

Another effect to be mentioned is that larger spin-orbit couplings are known to occur for Co-atoms with low coordination on terraces or along steps on Pt-surfaces.⁴⁰ Such an effect in principle can further enhance PMA in nanoclusters because of the flat cluster shape. However, because of strong Pt surface segregation in the nanoclusters most of the near-surface Co-atoms are buried in the second layer or have high coordination. Hence we expect that the few Co-atoms found in the outermost layer need not be treated separately.

Next we turn to analyzing the L_{12} -ordering of clus-

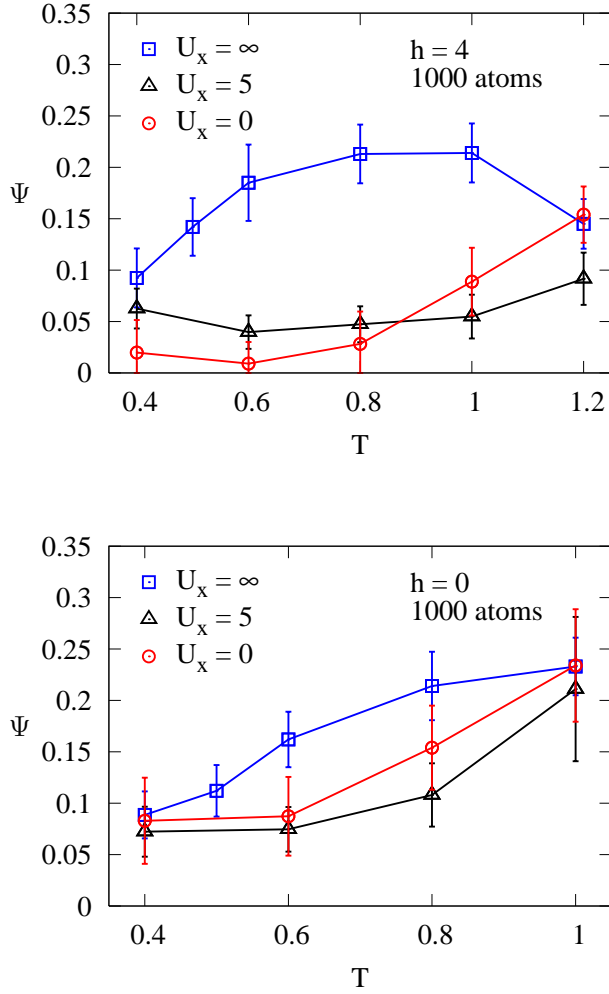


FIG. 8: Dependence of the order parameter for L1₂ structure Ψ on temperature for segregation controlling parameter $h = 4$ (upper panel) and $h = 0$ (lower panel). Values are averaged over 20 realizations for $h = 4$ and 10 realizations for $h = 0$.

ters. Analogous to experiments, we determine the L1₂ order parameter from the magnitudes of scattered intensities around the associated three superstructure peaks \mathbf{K}_i , $i = 1, 2, 3$ in reciprocal space. For that purpose, atoms of the cluster and the surrounding vacancies are represented by pseudo-spins $s_l \in \{1, 0, -1\}$ at the lattice positions \mathbf{R}_l with $s_l = 0$ for vacancies and $s_l = \pm 1$ for A and B , respectively. The structure factor is then calculated from the amplitudes $F_{\mathbf{k}} = \sum_l s_l e^{-i\mathbf{k} \cdot \mathbf{R}_l}$ which account for both the atomic arrangement in the cluster and the cluster shape. The finite dimensions of the cluster lead to a significant broadening of peaks in Fourier space, especially in the vertical direction. In order to account for this broadening, an integration in \mathbf{k} -space was performed around each peak in form of a sphere with radius $0.1/a$. The total scattering intensity is calculated as $I = \sum_{i=1}^3 \sum_{|\mathbf{k}-\mathbf{K}_i| < 0.1/a} |F_{\mathbf{k}}|^2$. As an order parameter

we define

$$\Psi = \frac{I - I_{\text{random}}}{I_{L1_2} - I_{\text{random}}} \quad (10)$$

Here I_{L1_2} and I_{random} are the intensities of clusters with identical shape, but perfect L1₂ order and random occupation by A and B atoms, respectively.

Fig. 8 shows the temperature dependent order parameter Ψ in cases of a strong surface field $h = 4$ (a) and $h = 0$ (b). The inclusion of exchange processes ($U_x < \infty$) diminishes Ψ due to reduced ordering through segregation effects. This can be understood from the large energy a Co adatom gains when it is incorporated by an exchange process into deeper layers of the cluster irrespective of its contribution to ordering.

In the presence of exchange processes we notice from the figures that ordering sets in at temperatures near $T \simeq 0.8$ to 1 (420 – 523 K). In experiments, the onset of L1₂ ordering was found for temperatures near 423 K for 3 nm thick films consisting of a dense assembly of islands.⁶ This temperature range is somewhat lower but close to the corresponding range in the simulations.

Comparison with Fig. 7 shows that PMA for $U_x = 5$ starts to decrease for $T \gtrsim 1$, which coincides with the onset of L1₂ ordering. One should bear in mind, however, that PMA in clusters is a surface induced effect and its decrease is caused by the change in cluster shape rather than by the concomitant bulk ordering.

To better visualize the statistics of growth, we present in Fig. 9 the layer-resolved evolution of one cluster. One can see pronounced incubation periods, before a nucleation event on top of the last layer takes place. Such an event is accompanied by a rapid initial growth and completion of the newly formed layer, followed by a period

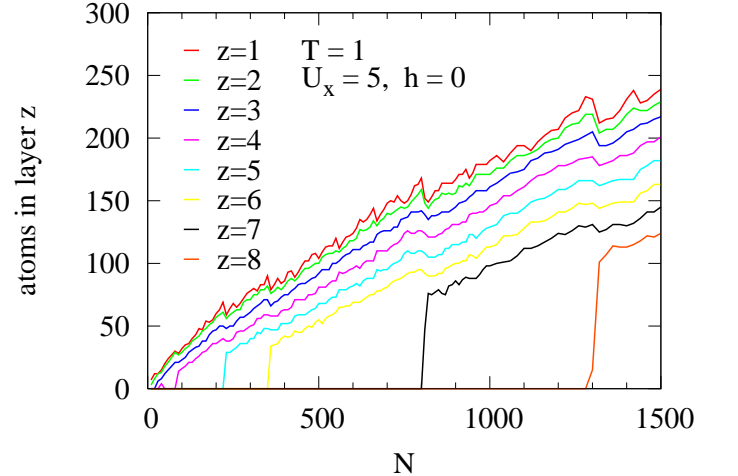


FIG. 9: Atoms per layer versus total number of atoms during the growth of one cluster. The curve on top shows the number of atoms in the first layer above the substrate and curves below represent successive layers on top. For the 4th to 8th layer nucleation events are visible as a strong initial increase in the number of atoms.

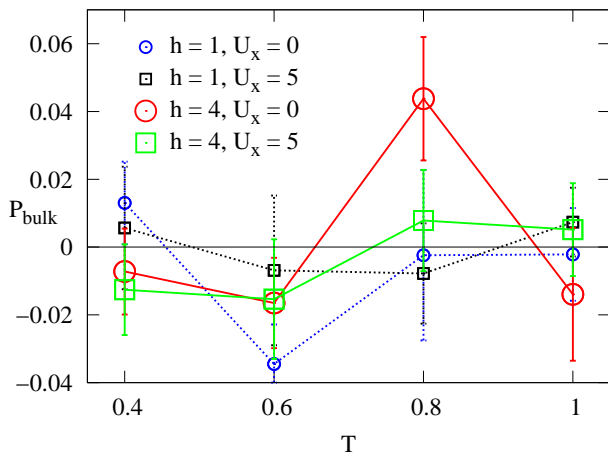


FIG. 10: Anisotropy parameter P_{bulk} for films as a function of temperature for different values of the exchange energy barrier U_x and surface field h . The error bars are calculated from the statistical error after averaging over 5 realizations of the growth process and the fit uncertainty (P as a function of $1/N$, see text) with error propagation.

of essentially lateral growth of the whole cluster without change in height. The slope in the atom numbers of the top layer immediately after nucleation is much higher than one. This means that most of the atoms incorporated in a new layer during its completion arrive through mass transport along the side facets, leading to a transient lateral shrinkage of all the layers below the growing top layer. This is seen in the figure by the small dips in all curves occurring simultaneously during the short time intervals when the top layer is filled.

The nucleation events on top can be described by a theory originally devised for second layer nucleation.⁴¹ This theory describes nucleation in a confined geometry with an influx of particles through deposition and loss of particles over a step edge. An essential parameter is the Schwoebel barrier that atoms have to surmount when crossing the step edge. In our simulations, this extra energy barrier effectively is about $\Delta E_s = V_0$ because the intermediate state for a transition from the top facet to a side facet has one bond less than adatoms with coordination three on the top surface. With the parameters typically used in the simulations, the fluctuation dominated regime III discussed in Ref. 41 is the relevant one for critical nuclei of size $i = 1, 2$. However, with the extra influx of atoms from the side facets, it is likely that the mean number of adatoms on top of the facet satisfies $\bar{n} > i$, so that mean-field theory may become justified for top layer nucleation.⁴¹

IV. FILMS

The same model is now applied to continuous films. We simulate the growth of films starting with an empty

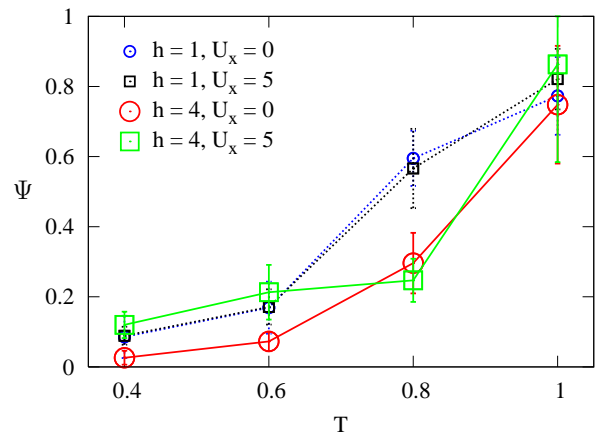


FIG. 11: Long range order parameter Ψ for films as a function of temperature for different values of the exchange energy barrier U_x and surface field h . Values are averaged over 5 realizations of the growth process.

simulation box with 224 atoms per layer and simulate growth up to deposition of 29 layers. The surface binding energy of $V_s = 3V_0 = -15$ induces film instead of cluster growth. As before, the surface binding is independent of the atom type so that segregation to the substrate similar to a free surface can be observed. Consequently, true bulk properties are only found a few layers above the substrate and below the top surface. In order to separate the bulk contribution from surface effects, we considered each realization of the growth process in the range of 2000 to 6500 atoms and made a linear fit of P vs. $1/N$. The anisotropy parameter in the bulk P_{bulk} is then found by extrapolating $N \rightarrow \infty$.⁴³ Fig. 10 shows the temperature dependence of the anisotropy parameter P_{bulk} for different values of U_x and h . For most sets of parameters, $P_{\text{bulk}} < 0$, i.e. Co-Pt bonds align preferentially in the film plane. However, for certain combinations of parameters, the simulations yield $P_{\text{bulk}} > 0$, supporting PMA.

Clearly, even if $P_{\text{bulk}} > 0$ it is too small to account for the measured PMA in thick CoPt_3 films at elevated temperatures. As shown recently, those measurements can be explained by a model with interatomic interaction potentials that depend on the coordination of the atoms involved.¹⁷ One essential feature of this model is that an effective segregation parameter, related to h in our model, changes sign for intermediate coordinations of Co-atoms and thus favors Co segregation towards step edges in the surface. This sign change of h , however, should not significantly affect our conclusions. There we focused on the temperature range $T \lesssim 1$, where Co-segregation according to Ref. 17 ceases to be effective.

The degree of long-range order in films is shown in Fig. 11 at temperatures below the transition temperature $T_0 \simeq 1.83$, where bulk kinetics are suppressed. With higher T , the order parameter Ψ becomes larger. Similar to our findings for clusters, the order parameter Ψ in the

case $h = 4$ is suppressed relative to $h = 1$, as clearly seen from the data at $T = 0.8$. Surface segregation therefore appears to impede the development of long range order.

V. CONCLUSIONS

In order to study growth kinetics of binary alloys we developed a lattice model based on nearest neighbor bonds with bond energies chosen to match equilibrium properties of CoPt₃. The kinetic parameters were obtained from diffusion experiments,¹³ DFT calculations,⁴² and in addition from experiments observing interatomic exchange processes in the Co/Pt system.^{26,44}

Experiments on CoPt₃ nanoclusters on a weakly binding substrate⁷ have revealed PMA in a temperature window that is well reproduced by our simulations. This temperature range is bounded towards low temperatures by frozen-in surface kinetics. The disappearance of PMA at higher temperatures is explained by the interplay of Pt surface segregation facilitated by direct exchange processes, and a transition from oblate to spherical cluster shapes. Our analysis suggests that the transition is not caused by L1₂ ordering. Yet, in our simulations the onset of L1₂ ordering is detected in the same temperature range where PMA disappears, in qualitative agreement with the measurements. It should be noted that up to $T \simeq 1$ long range order is induced solely by surface processes, as the bulk kinetics remain still frozen.

The structural anisotropy responsible for the magnetic anisotropy is characterized in our model primarily by a difference in the numbers of Co-Pt bonds out-of-plane and in-plane. Within a bond picture each Co-Pt bond provides a local contribution to the magnetic anisotropy, which tends to align the Co-moment parallel to the bond. An associated magnetic bond energy, deduced from experiments on Co-Pt multilayers, can reasonably reproduce the magnitude of PMA measured for nanoclusters in the appropriate temperature range. PMA is predicted to be a surface effect, a feature which could be tested experimentally.

Dipolar interactions tend to turn the easy axis of magnetization into the plane. The two competing effects,

bond anisotropy (surface term) and dipolar interactions (volume term), lead to an optimum cluster size where the anisotropy energy of a cluster is largest, and a second characteristic size where PMA disappears.

The importance of cluster shape effects revealed by our computations is also corroborated by experiment, where a rotation of the easy magnetization axis into the film plane and an associated change in the aspect ratio from oblate to prolate was found in separate measurements on cluster assemblies at higher coverages.⁶ In our simulations, we observed clusters to become more spherical in shape and to develop an excess of in-plane Co-Pt bonds with increasing temperature.

Application of the same methodology to growing continuous films yields a bulk structural anisotropy favoring in-plane magnetization for most of the parameters studied. However, it can yield a positive bulk contribution to P^{CoPt} in a certain temperature range provided direct exchange processes are sufficiently fast. The associated PMA, however, is quite small and disappears for $T \gtrsim 1$. At these higher temperatures a different mechanism has been proposed recently to describe PMA in thick films in terms of in-plane Co clustering.¹⁷

Finally, we like to draw attention to the question of growth of magnetic clusters or films in strong external magnetic fields that saturates the magnetization in the growth direction. The magnetic anisotropy energy should then induce an anisotropy in the probabilities for atomic hopping such that out-of-plane Co-Pt bonding and PMA become favored. In fact, simulation results for growth in a magnetic field suggest that this effect might become detectable in the Co-Pt system. In particular, for L1₀ ordered alloys estimates based on Landau theory suggest that this additional field-induced PMA becomes stronger.⁴⁵

Acknowledgments

We thank M. Albrecht, M. Einax, M. Kessler, A. Majhofer and G. Schatz for helpful discussions. This work was supported in part by the Deutsche Forschungsgemeinschaft (SFB 513).

¹ J. A. Venables, G. D. T. Spiller, and M. Hanbücken, Rep. Prog. Phys. **47**, 399 (1984).

² J. Rottler and P. Maass, Phys. Rev. Lett. **83**, 3490 (1999).

³ S. Heinrichs, J. Rottler, and P. Maass, Phys. Rev. B **62**, 8338 (2000).

⁴ H. Brune, Surf. Sci. Rep. **31**, 121 (1998).

⁵ T. Michely and J. Krug, *Islands, Mounds and Atoms* (Springer, Berlin, Heidelberg, 2004).

⁶ M. Albrecht, M. Maret, A. Maier, F. Treubel, B. Riedlinger, U. Mazur, G. Schatz, and S. Anders, J. Appl. Phys. **91**, 8153 (2002).

⁷ M. Albrecht, A. Maier, F. Treubel, M. Maret, P. Poinso,

and G. Schatz, Europhys. Lett. **56**, 884 (2001).

⁸ A. L. Shapiro, P. W. Rooney, M. Q. Tran, F. Hellman, K. M. Ring, K. L. Kavanagh, B. Rellinghaus, and D. Weller, Phys. Rev. B **60**, 12826 (1999).

⁹ H. Zeng, J. Li, J. P. Liu, Z. L. Wang, and S. Sun, Nature **420**, 395 (2002).

¹⁰ G. Andersson, T. Burkert, P. Warnicke, M. Björck, B. Sanyal, C. Chacon, C. Zlotea, L. Nordström, P. Nordblad, and O. Eriksson, Phys. Rev. Lett. **96**, 037205 (2006).

¹¹ Y. Gauthier, R. Baudouin-Savois, J. M. Bugnard, U. Bardi, and A. Atrei, Surf. Sci. **276**, 1 (1992).

¹² J. M. Sanchez, J. L. Morán-López, C. Leroux, and M. C.

- Cadeville, J. Phys.: Condens. Matter **1**, 491 (1989).
- ¹³ M. Bott, M. Hohage, M. Morgenstern, T. Michely, and G. Comsa, Phys. Rev. Lett. **76**, 1304 (1996).
 - ¹⁴ M. T. Johnson, P. J. H. Bloemen, F. J. A. den Broeder, and J. J. de Vries, Rep. Prog. Phys. **59**, 1409 (1996).
 - ¹⁵ S. Heinrichs, W. Dieterich, and P. Maass, Europhys. Lett. **75**, 167 (2006).
 - ¹⁶ A.-L. Barabási and H. E. Stanley, *Fractal concepts in surface growth* (Cambridge University Press, Cambridge [a.o.], 1995).
 - ¹⁷ B. B. Maranville, M. Schuerman, and F. Hellman, Phys. Rev. B **73**, 104435 (2006).
 - ¹⁸ J. O. Cross, M. Newville, F. Hellman, P. W. Rooney, A. L. Shapiro, and V. G. Harris, J. Synchrotron Rad. **8**, 880 (2001).
 - ¹⁹ P. Kratzer, E. Penev, and M. Scheffler, Appl. Phys. A **75**, 79 (2002).
 - ²⁰ M. Kessler, W. Dieterich, and A. Majhofer, Phys. Rev. B, **67**, 134201 (2003); *ibid* **64**, 125412 (2001).
 - ²¹ H. Berg and J. B. Cohen, Metall. Trans. **3**, 1797 (1972).
 - ²² K. Binder, Phys. Rev. Lett. **45**, 811 (1980).
 - ²³ P. J. Feibelman, Surf. Sci. **423**, 169 (1999).
 - ²⁴ E. Kentzinger, V. Parasote, V. Pierron-Bohnes, J. F. Lami, M. C. Cadeville, J. M. Sanchez, and R. Caudron, Phys. Rev. B **61**, 14975 (2000).
 - ²⁵ M. De Santis, R. Baudoing-Savois, P. Dolle, and M. C. Saint-Lager, Phys. Rev. B **66**, 085412 (2002).
 - ²⁶ P. Gambardella, M. Blanc, L. Burgi, K. Kuhnke, and K. Kern, Surf. Sci. **449**, 93 (2000).
 - ²⁷ G. L. Kellog, Surf. Sci. Rep. **21**, 1 (1994).
 - ²⁸ F. Menzinger and A. Paoletti, Phys. Rev. **143**, 365 (1966).
 - ²⁹ M. L. Néel, J. de Phys. et le Radium **15**, 225 (1954).
 - ³⁰ R. H. Victoria and J. M. MacLaren, J. Appl. Phys. **73**, 6415 (1993).
 - ³¹ J. B. Staunton, S. S. A. Razee, M. F. Ling, D. D. Johnson, and F. J. Pinski, J. Phys. D **31**, 2355 (1998).
 - ³² D. Weller, R. F. C. Farrow, R. F. Marks, G. R. Harp, H. Notarys, and G. Gorman, Proc. Materials Research Society **313**, 791 (1993).
 - ³³ N. W. E. McGee and M. T. Johnson, J. Appl. Phys. **73**, 3418 (1993).
 - ³⁴ J. V. Harzer, B. Hillebrands, R. L. Stamps, G. Güntherodt, D. Weller, C. Lee, R. F. C. Farrow, and E. E. Marinero, J. Magnet. Magn. Mater. **104–107**, 1863 (1992).
 - ³⁵ S. S. A. Razee, J. B. Staunton, B. Ginatempo, E. Bruno, and F. J. Pinski, Phys. Rev. B **6401**, 014411 (2001).
 - ³⁶ The value for A^{CoPt} can be afflicted with uncertainty arising from measurements of films with varying interface quality through different preparation methods. In a previous work¹⁵ we estimated this parameter based on experiments with values K^{CoPt} falling in the range^{33,34} of 0.27–1.15 mJ/m². The model can also describe the major contribution of the anisotropy resulting from alternating Pt and Co atomic layers in the ordered L1₀-phase of CoPt, where the lattice distortion (tetragonalization) is only responsible for about 20% of the observed anisotropy.³⁵
 - ³⁷ J. Kohlhepp and U. Gradmann, J. Magnet. Magn. Mater. **139**, 347 (1995).
 - ³⁸ P. Beauvillain, A. Bounouh, C. Chappert, R. Megy, S. Ouldmafhoud, J. P. Renard, P. Veillet, D. Weller, and J. Corno, J. Appl. Phys. **76**, 6078 (1994).
 - ³⁹ R. Wu, C. Li, and A. J. Freeman, J. Magnet. Magn. Mater. **99**, 71 (1991).
 - ⁴⁰ P. Gambardella, S. Rusponi, T. Cren, N. Weiss, and H. Brune, Comptes Rendus Physique **6**, 75 (2005).
 - ⁴¹ S. Heinrichs and P. Maass, Phys. Rev. B **66**, 073402 (2002).
 - ⁴² P. J. Feibelman, Phys. Rev. B **60**, 4972 (1999).
 - ⁴³ An alternative determination of P_{bulk} where the outermost two layers at the top and bottom are excluded yields comparable results. We defined the outermost two layers to consist of atoms with coordination less or equal to 11 together with their nearest neighbors.
 - ⁴⁴ E. Lundgren, B. Stanka, W. Koprolin, M. Schmid, and P. Varga, Surf. Sci. **423**, 357 (1999).
 - ⁴⁵ M. Einax, S. Heinrichs, P. Maass, A. Majhofer, and W. Dieterich, Materials Science and Engineering: C (Proceedings of the E-MRS 2006 Spring Meeting).